J Solid State Electrochem (2009) 13:1321–1326
DOI 10.1007/s10008-008-0669-1

ORIGINAL PAPER

Synthesis and growth mechanism of zirconia nanotubes by anodization in electrolyte containing Cl^-

Limin Guo · Jianling Zhao · Xixin Wang · Rongqing Xu · Yangxian Li

Received: 20 May 2008 / Revised: 31 July 2008 / Accepted: 31 July 2008 / Published online: 30 September 2008

Abstract The formation and growth of a self-organized zirconia porous layer can be achieved directly by anodization of Zr in chloride containing electrolytes. The morphology of the porous layers is affected by electrochemical conditions such as Cl^- concentration. Zirconia nanotubes with diameters ranging from 250 to 300 nm and a length of 33 μm were formed under proper conditions. The nanotubes have smooth and straight walls. The composition of the nanotubes was characterized by using an energy dispersive spectrometer. Selected area electron diffraction investigation reveals that the as-anodized zirconia nanotubes have an amorphous structure. Crystal phase transition and structural stability of the ZrO_2 nanotubes after heat treatment were characterized. A possible growth mechanism is presented.

Keywords Zirconia · Nanotube · Anodization · HCl

Introduction

Zirconia has been widely used as a structural ceramic material [1, 2], catalyst or catalyst support [3, 4], sensor [5, 6], solid electrolyte [7], etc. In particular, zirconia (ZrO_2) nanotubes have generated a lot of interest because of their unique physical and chemical properties. They are significantly different from their microcrystalline counterparts [8–10] due to their enhanced surface area to volume ratio, quantum confinement, and changes in the lattice parameters [11]. There were many researches which focus on the synthesis of zirconia nanotubes using the templating technique [12–14] or hydrothermal method [15]. Self-organized zirconia nanotubes prepared by electrochemical processes have also attracted much interest in the past several years owing to their importance in basic scientific research, potential technology applications, and precise control of critical electrochemical process parameters, such as the anode voltage, time, and compositions of electrolyte [16–19]. However, all anodically fabricated ZrO_2 nanotubes reported to date had fluorine present in the electrolyte [16–22]. It has been hypothesized that fluorine ions are essential and perhaps a unique ingredient for the formation of nanoporous or nanotubular ZrO_2 because of the formation of complex ZrF_6^{2-} in solution [23, 24]. To the best of our knowledge, there were no reports about the preparation of zirconia nanotubes in Cl^--containing electrolyte.

In this paper, formamide (FA) and glycerol (GE; volume ratio 1:1) electrolytes containing 0.5–5 wt.% HCl were used to prepare zirconia nanotubes by electrochemical method. High-aspect-ratio ZrO_2 nanotubes were obtained under the appropriate HCl concentration. A possible growth mechanism and electrochemical reactions are presented.

Experimental

In this work, zirconium foil samples (10 mm×7 mm×0.5 mm) with a purity of 99.7% were obtained from

L. Guo · J. Zhao · R. Xu · Y. Li
School of Material Science and Engineering,
Hebei University of Technology,
Tianjin 300130, China

J. Zhao (✉) · Y. Li (✉)
8 Guangrong Road,
Tianjin City 300130, China
e-mail: hebutzhaoj@126.com
e-mail: yxli@mail.hebut.edu.cn

X. Wang
School of Chemical Engineering and Technology,
Hebei University of Technology,
Tianjin 300130, People's Republic of China

General Research Institute for Nonferrous Metals (Beijing, China). Before the experiments, the samples were rinsed and sonicated in acetone, ethanol, and deionized (DI) water, and then dried in the air. The electrochemical cell consisted of two electrodes with zirconium foil as anode and Pt foil (20 mm×20 mm×0.1 mm) as counter electrode. The distance between anodic and cathodic electrodes was 25 mm. Electrolytes in this process were formamide and glycerol (volume ratio 1:1) containing 0.5–5 wt.% HCl and 3.5 wt.% H_2O. All the electrolytes were prepared from analytical grade chemicals. Electrochemical treatment potential was 20 V supplied by a high-voltage direct current potentiostat (TPR25024, Dahua Coop, Beijing, China) and swept from an open-circuit potential (OCP) to 20 V with a sweep rate of 0.1 V/s, followed by holding the potential at 20 V for 5 h. This slow voltage sweep procedure can obtain

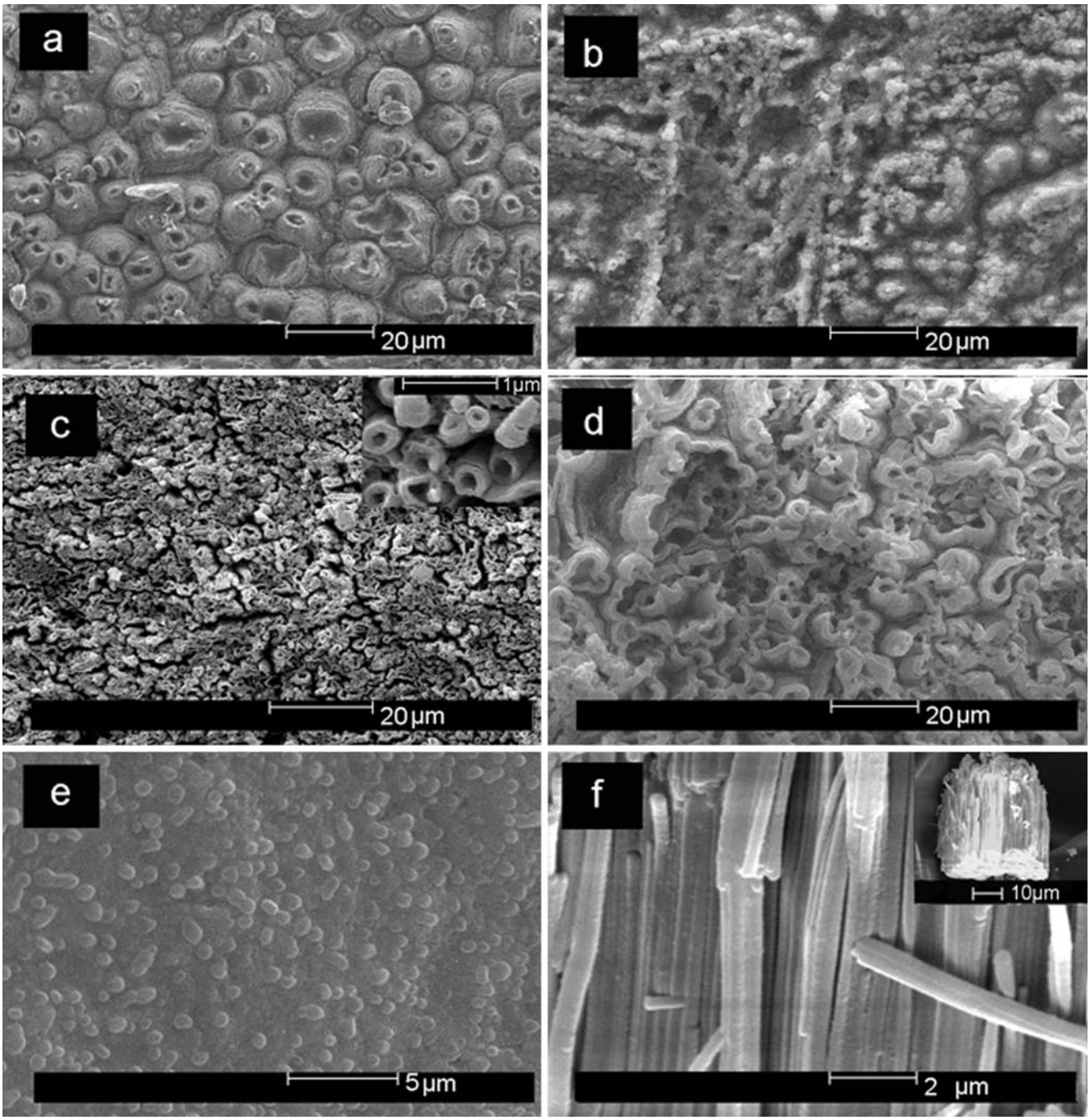

Fig. 1 SEM images of the anodized samples in different HCl concentration at 20 V for 5 h: *surface view* in **a** 0.5 wt.% HCl, **b** 1 wt.% HCl, **c** 2 wt.% HCl, **d** 5 wt.% HCl; **e** *bottom view* and **f** cross-section of (**c**)

a more regular surface morphology than putting the voltage directly at 20 V. A similar behavior was reported by Tsuchiya et al. [24, 25].

After being removed from the anodizing solution, the samples were cleaned in ethanol and DI water and then dried and characterized. The microstructure of the specimens before and after heat treatment was carefully examined by a scanning electron microscope (SEM Philips XL 30). The specimens for transmission electron microscope (TEM, Philips Tecnai 20) were prepared by scratching the nanotubal layer with a sharp tool, then sonicated in ethanol and observed on a carbon-coated copper grid. The elemental composition and phase structure of the resulting nanotubes were analyzed using energy dispersive spectrometer (EDS) and X-ray diffraction (XRD) on a D/MAX2500PC diffractometer (Rigaku Japan) with Cu Kα radiation, respectively.

Results and discussion

Figure 1a–d shows the surface morphologies of the samples after anodizing for 5 h in FA + GE (volume ratio 1:1) electrolytes containing 0.5–5 wt.% HCl. Oxidizing zirconium in electrolyte containing 0.5 wt.% HCl resulted in a compact zirconia layer with volcanical knobs on the surface. These knobs have sizes of 10–20 μm (Fig. 1a). After anodization in electrolyte containing 1 wt.% HCl, the surface of the zirconia layer appears to be rough with a few pores displaying in a partial area (Fig. 1b). In 2 wt.% HCl electrolyte, nanopores with discrete, hollow, and cylindrical features are formed over the substrate (Fig. 1c). The inner diameters of the pores are 200–250 nm as shown in high magnification in Fig. 1c. A cabbage-like surface morphology is observed on the zirconia layer fabricated under 5 wt.% HCl concentration (Fig. 1d). It can be seen that the pores overlap together and become wide and irregular.

From the SEM images, it indicates that the 2 wt.% HCl concentration is an appropriate one for the preparation of zirconia nanotubes in this experiment. Bottom and cross-section views were obtained from a mechanically cracked oxide film after anodization in 2 wt.% HCl electrolyte (Fig. 1e,f), where some pieces lie upside down. It can be seen that densely packed nanotubes are synthesized in such electrolyte (Fig. 1f). The closed and dome-like bottom is apparently a barrier oxide layer (Fig. 1e). Lateral image (Fig. 1f) of the nanotube reveals that these nanotubes possess smooth and straight walls with an outer diameter of about 250–300 nm and a length of 33 μm. A big diameter may facilitate their use as a catalyst, chemical sensor, and host container that may be filled with other materials and inert chamber for chemical reactions [16].

Elemental composition of the nanotubes formed in 2 wt.% HCl electrolyte is confirmed by EDS. The result (Fig. 2) shows that besides zirconium (Zr) and oxygen (O), chlorine (Cl), gold (Au), and carbon (C) were also present in these nanotubes. Chlorine was detected because the remnant solute (HCl) had not been completely eliminated. The carbon was detected due to the organic solvent used in the experiment and contamination of instruments, while the Au was detected due to the gold coating of the samples.

For a more detailed microstructural characterization, TEM investigations were carried out for the cross-section

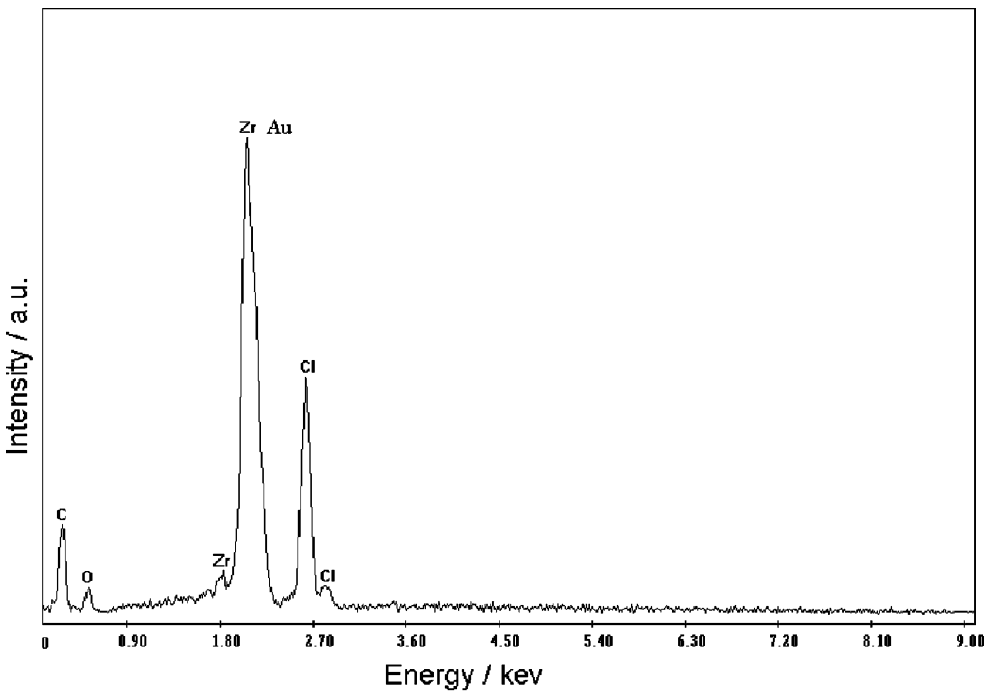

Fig. 2 EDS spectrum of the zirconia nanotubes prepared in 2 wt.% HCl electrolyte

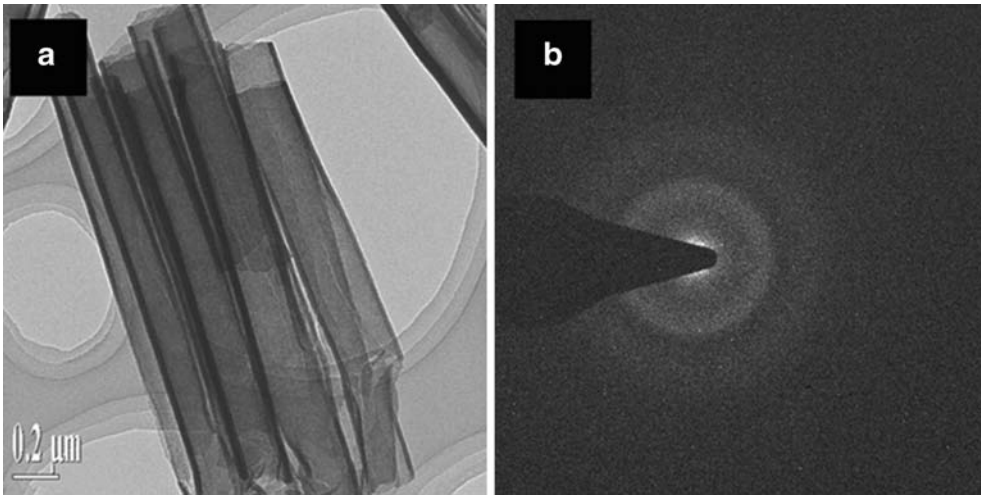

Fig. 3 TEM image (**a**) and selected area diffraction pattern (**b**) of zirconia nanotubes formed in FA + GE (volume ratio 1:1) containing 2 wt.% HCl

view of the sample anodized in 2 wt.% HCl electrolyte at 20 V for 5 h. As seen in Fig. 3a, straight and hollow nanotubes are revealed, showing almost the same wall thickness. The diameter of the nanotubes is about 250–300 nm. Figure 3b is a selected area electron diffraction pattern of the zirconia nanotubes, indicating the amorphous structure of the as-anodized nanotubes.

Figure 4 is the cross-sectional view of the zirconia nanotube arrays obtained in 2 wt.% HCl and annealed at 400 and 800 °C. Compared with the as-prepared nanotubes (Fig. 1f), the microstructure of the sample changes slightly after annealing at 400 °C (Fig. 4a). At 800 °C, the nanotubal structure had a little collapse and cracks (Fig. 4b) and some hubble-like particles with sizes of 1–2 μm were observed on the walls. These may be due to the phase transformation and volume expansion in the nanotubes during heat treatment. X-ray diffraction analysis was taken to identify the crystalline phases that may be present in the zirconia nanotubes after annealing at 400 and 800 °C. The results are shown in Fig. 5. It is clear that after annealing at 400 and 800 °C, the amorphous oxide layer transformed to tetragonal ZrO_2 and monoclinic ZrO_2, respectively. As shown in Fig. 5a, peaks at 30.12°, 35.21°, 50.40°, and 60.20° correspond respectively to the (101), (110), (112), and (211) planes of tetragonal ZrO_2 (PDF card no. 79-1770). After annealing at 800 °C, the crystalline phase of the structure was predominantly monoclinic ZrO_2 (PDF card no. 37-1484) with a little tetragonal ZrO_2 (Fig. 5b).

Figure 6 is the current–time transients during anodization in different electrolytes for 5 h after a potential sweep from OCP to 20 V. As shown in the figure, all the curves went through three steps: a drastic drop at first (before 15 min), then a slow decrease during 15–150 min, and finally a steady state (after 150 min). This phenomenon has been found in several reports including titanium [17] and zirconium [21, 26]. Also, the concentration of HCl had a strong promoting effect on the current density (Fig. 6a–d). With increasing Cl^- concentration, the conductivity of the electrolyte enhanced and an additional dissolution process took place. Different oxide morphologies (Fig. 1a–d) were obtained corresponding to the different reaction rates in these electrolytes. Zirconia nanotubal structure can only be synthesized in a moderate HCl concentration (2 wt.%). When the HCl concentration was increased to 5 wt.%, the nanopores overlap together and become wide and irregular.

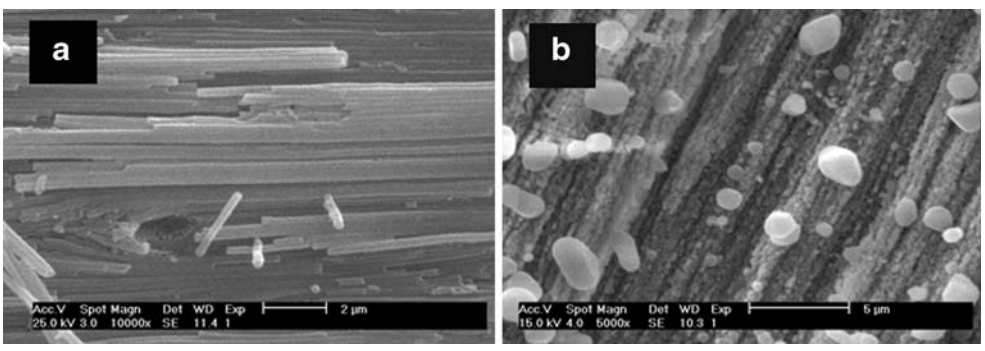

Fig. 4 SEM images of the anodized sample in 2 wt.% HCl and annealed at 400 (**a**) and 800 °C (**b**)

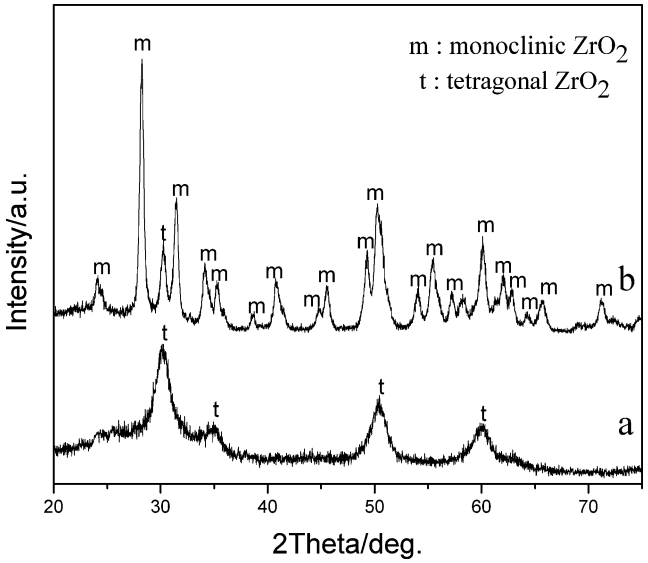

Fig. 5 XRD patterns of the samples obtained in 2 wt.% HCl electrolyte with annealing at 400 °C (*a*) and 800 °C (*b*)

This may result from the additional chemical dissolution of pore wall during anodization.

From the current–time curves, the growth mechanism of the ZrO_2 nanotube can be divided into three stages. (1) formation of ZrO_2 film at the surface of zirconium: oxide grows at the surface of the metal due to the interaction of metallic cations with O^{2-} and OH^- coming from H_2O [27]. This reaction happens with a high speed which can be confirmed by the big current at the beginning of anodization (Fig. 6). Then with the growing of the oxide layer, resistance increases and reaction speed decreases. So, a drastic drop of current happens. The overall reactions are represented as:

$$Zr \rightarrow Zr^{4+} + 4e^- \quad (1)$$

$$Zr^{4+} + 2H_2O \rightarrow ZrO_2 + 4H^+ \quad (2)$$

(2) Field-assisted dissolution of the oxide as soluble chloride complexes at the oxide/electrolyte interface: With the generation of the ZrO_2 film, the volume must expand at the surface of the metal substrate due to the participation of O atoms into Zr. Then volume stress becomes higher and reaction heat becomes more difficult to be released. In order to lower the internal energy, a large number of microcracks arise on the oxide/electrolyte interface. At the same time, selective dissolution takes place due to electric field and the microcracks on the oxide layer [28]. Because of the occurrence of microcracks, the electric field distribution within the oxide film changes. Especially, at the bottom of the cracks, field increases greatly. As a result, the concentrations of anions, such as Cl^-, O^{2-}, and OH^- increase because of electrostatic attraction. So, it turns easier for ZrO_2 to dissolve into the electrolyte at the bottom of the cracks. Then, small pits are formed on the surface of the layer. This reaction of electrochemical dissolution can be described below:

$$ZrO_2 + 6Cl^- + 4H^+ \rightarrow [ZrCl_6]^{2-} + 2H_2O \quad (3)$$

(3) Deepening of the pores on oxide layer: small pits originating from this oxide layer make the barrier layer at the bottom of the pits relatively thinner than at the wall. On the one hand, these pits increase the electric field intensity across the remaining barrier layer, resulting in their further expansion. On the other hand, they provide an easier pathway for more O^{2-} or OH^- to migrate through the barrier layer, leading to further metal oxidization. So, corrosion pits grow up with time. In this stage, the rate of current decrease being retarded may result from the formation of the corrosion pits [28]. The growing of pores is related to the forming of oxide film at the metal/oxide interface and electrochemical dissolution of oxide film at the oxide/electrolyte interface of the pore bottom. When the chemical dissolution and electrochemical etching speed are too large or too small compared to the oxide formation, the ZrO_2 nanotubes cannot be formed. There exists a stable equilibrium between the formation and dissolution of the oxide, where the current maintains a steady value.

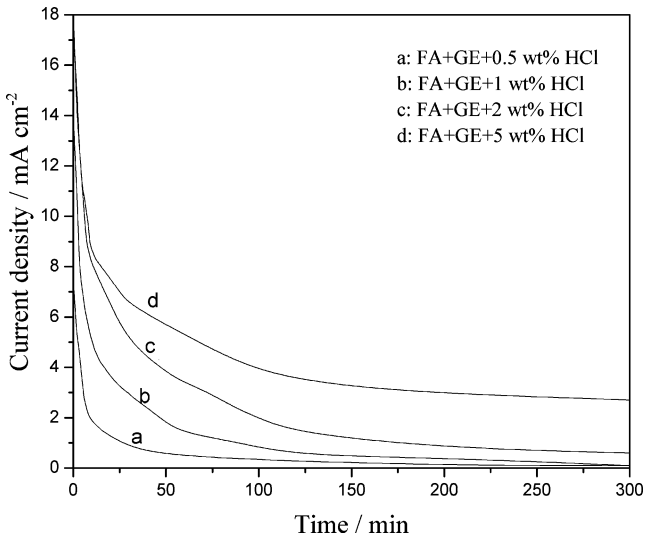

Fig. 6 Current–time curves for the anodization of Zr in different HCl concentrations at 20 V for 5 h

Conclusion

Self-organized zirconia porous layers are fabricated by electrochemical anodization of zirconium in FA and GE

(volume ratio 1:1) electrolytes containing HCl. The morphology of the anodized oxide layer changes remarkably along with the changing of HCl concentrations. After anodization in 2 wt.% HCl for 5 h at 20 V, zirconia nanotubes with a diameter ranging from 250 to 300 nm and a length of 33 μm were formed. The as-grown zirconia nanotubes have an amorphous structure. After annealing at 400 and 800 °C, this amorphous zirconia nanotube layer transformed to tetragonal ZrO_2 and monoclinic ZrO_2, respectively. Furthermore, the possible reactions during the formation of the nanotubes are revealed too.

Acknowledgments This work is supported by Tianjin Natural Science Foundation (07JCYBJC03300), the Key Project of Chinese Ministry of Education (No. 208013), and the Natural Science Foundation of Hebei Province of China (E2007000044).

References

1. Schroeder V, Ritchie RO (2006) Acta Mater 54:1785 doi:10.1016/j.actamat.2005.12.006
2. Santos C, Maeda LD, Cairo CAA, Acchar W (2008) Int J Refract Met Hard Mater 26:14 doi:10.1016/j.ijrmhm.2007.01.008
3. Hyun CL, Doohwan L, Ok YL, Soonho K, Yong TK et al (2007) Stud Surf Sci Catal 167:201 doi:10.1016/S0167-2991(07)80132-7
4. Liu XM, L GQ, Yan ZF (2005) Appl Catal A: Gen 279:241 doi:10.1016/j.apcata.2004.10.040
5. Lvov SN, Zhou XY, Ulmer GC, Barnes HL et al (2003) Chem Geol 198:141 doi:10.1016/S0009-2541(03)00033-0
6. Spirig JV, Ramamoorthy R, Akbar SA, Routbort JL et al (2007) Sens Actuators B Chem 124:192 doi:10.1016/j.snb.2006.12.022
7. Noriya I, Woosuck S, Ichiro M, Norimitsu M et al (2005) Sens Actuators B Chem 108:216 doi:10.1016/j.snb.2004.11.034
8. Limaye AU, Helble JJ (2004) Aerosol Sci 35:599 doi:10.1016/j.jaerosci.2003.11.008
9. Edelstein AS (1996) Nanomaterials: synthesis, properties and application. Institute of Physics Publication, London
10. Mueller R, Jossen R, Pratsinis SE (2004) J Am Ceram Soc 87:197 doi:10.1111/j.1551-2916.2004.00197.x
11. Tok AIY, Boey FYC, Du SW, Wong BK (2006) Mat Sci Eng B-Solid 130:114 doi:10.1016/j.mseb.2006.02.069
12. Xu H, Qin DH, Yang Z, Li HL (2003) Mater Chem Phys 80:524 doi:10.1016/S0254-0584(03)00002-6
13. Melezhyk OV, Prudius SV, Brei VV (2001) Microporous Mesoporous Mater 49:39 doi:10.1016/S1387-1811(01)00397-3
14. Signoretto M, Breda A, Somma F, Pinna F, Cruciani G (2006) Microporous Mesoporous Mater 91:23 doi:10.1016/j.micromeso.2005.11.004
15. Monty C, Millers D (2005) Sens Actuators B Chem 109:102 doi:10.1016/j.snb.2005.03.092
16. Lee WJ, Smyrl WH (2005) Electrochem Solid-State Lett 8:B7 doi:10.1149/1.1857115
17. Yasuda K, Schmuki P (2007) Electrochim Acta 52:4053 doi:10.1016/j.electacta.2006.11.023
18. Zhao JL, Xu RQ, Wang XX, Li YX (2008) Corros Sci. doi:10.1016/j.corsci.2008.01.026
19. Tsuchiya H, Schmuki P (2004) Electrochem Commun 6:1131 doi:10.1016/j.elecom.2004.09.003
20. Yasuda BK, Schmuki P (2007) Adv Mater 19:1757 doi:10.1002/adma.200601912
21. Tsuchiya H, Macak JM, Taveira L, Schmuki P (2005) Chem Phys Lett 410:188 doi:10.1016/j.cplett.2005.05.065
22. Xu RQ, Zhao JL, Tao JL, Lu ZM, Li YX (2008) Key Eng Mat 1510:368–372
23. Richter C, Wu Z, Panaitescu E, Willey RJ, Menon L (2007) Adv Mater 19:946 doi:10.1002/adma.200602389
24. Tsuchiya H, Macak JM, Ghicov A, Taveira L, Schmuki P (2005) Corros Sci 47:3324 doi:10.1016/j.corsci.2005.05.041
25. Tsuchiya H, Macak JM, Sieber I, Schmuki P (2005) Small 7:722 doi:10.1002/smll.200400163
26. Tsuchiya H, Macak JM, Sieber I, Schmuki P (2006) Mater Sci 512:205
27. Gong D, Grimes CA, Varghese OK (2001) J Mater Res 16:3331 doi:10.1557/JMR.2001.0457
28. Zhao JL, Wang XH, Chen RZ, Li LT (2005) Solid State Commun 134:705 doi:10.1016/j.ssc.2005.02.028